SOHO

CDS SOFTWARE NOTE No. 56

Version 1   12 January 2000

GIS CALIBRATION DETAILS

Eddie Breeveld
Mullard Space Science Laboratory
University College London
Holmbury St. Mary
Dorking
Surrey RH5 6NT
United Kingdom

erb@mssl.ucl.ac.uk

Revision list

Version 1, 2000/01/12	Original

Table of Contents

1. Introduction

This note describes the wavelength and intensity calibration of the GIS detectors, estimating errors where possible. The contribution of detector effects to the errors are also discussed.

Calibration and corrections are performed by three IDL software routines in the GIS analysis software, which will be discussed in detail:

`gis_smooth`	for fixed patterning;
`ghost_buster`	for ghosting;
`gis_calib`	for electronic, geometric, flat field, and absolute calibrations.

The various methods for calling these procedures are not mentioned here, see instead the GIS Software User Manual.

1.1 Related Documents

This document is part of a set of 'software' notes describing the CDS instrument and associated analysis software. These are distributed as part of the CDS software IDL libraries, and can be found at *http://orpheus.nascom.nasa.gov/cds/software_notes.html* and a subset at *http://solg2.bnsc.rl.ac.uk/software_notes.html*. It is assumed that readers are familiar with the contents of these documents.

- CDS Software note 54: GIS Instrument Guide[1].
- CDS Software note 55: GIS Software User Manual[2].

Other relevant documentation can be found in the References section on page 25.

2. Wavelength Calibration

The best fits to the wavelength scale are quadratic. One fundamental reason is that the detectors are flat whereas the spectral axis is a curved Rowland circle, and the incident light is at a high grazing incidence angle; this leads to a quadratic error.

Another factor which has to be taken into account when considering the geometry is the way the lines are mapped onto the Rowland circle (RC). The arc length around the RC is not proportional to wavelength, but is proportional to the sine of the angle at which the light leaves the grating. This has the effect of partly compensating for the flatness of the detector, reducing the error from ±40 pixels to ±10 pixels. The mapping of the wavelength to pixels is demonstrated in Figure 1. The residuals are measured from a straight line crossing the RC at the same two points as the detector front face is designed to do.

The second reason is associated with the look-up table (LUT). The convolution of the charge cloud with the anode leads to a reduction in spiral radius, but the shrinkage is not proportional to radius. When a spiral is fitted to the output, the result is a spiral with fewer arms than in the anode design. Because the position of a spectral line in this polar plane only shifts in radius and not in angle, the line may appear on arm 3

rather than arm 5. This results in another quadratic error in the wavelength calibration, but this time dependent on the amount of shrinkage. It can easily be calculated if the LUT parameter *start* is known, and this is the method adopted.

Observations with different slits show a variation in the wavelength ranges of less than 1Å between slits 1 and 5. The ranges were, however, slightly different from expectation. This could be caused by small errors in the location of the detectors on the RC, or by rotation of the detectors themselves so that they are not perfectly tangential to the RC. A rotation of the grating could also have an effect. As the ranges still cover the prime lines the worst possibility is if the whole offset is caused by movement of the detectors along the RC radius because this would lead to the largest broadening of the line widths.

It was also noticed that there were shifts in the line positions with changes in slit, mirror and aperture position. Scanning the full aperture gave shifts of 3–5 pixels. This was also seen in the NIS. The shift implies a slight misalignment of the source and slits. The wavelength calibration has to depend on all these factors—slit number, slit and mirror position and the LUT *start* parameter.

2.1.1 Errors in Wavelength

There are many contributions to errors in the wavelength scales, fortunately the major divergences (as discussed above) are accounted for in the automatic wavelength conversion routines `wave2pix` and `pix2wave`. It is important to ensure that the correct calibration is used for each dataset, the routine `restore_wavecal` can be used to ensure this. Residual errors from these calibrations are most noticeable at the edges of the detectors (see section 5.3 below). Smaller variations (up to 20% of the line width) are possible, and come mainly from changes in the temperature of the GIS, and variations in the count rates. No automatic corrections are applied for these deviations. Other errors in the wavelength calibrations are discussed in the individual sections below.

3. Look-up Table corrections

There are two corrections needed for the on-board look-up table (LUT). One is fixed patterning, and the other ghosting.

3.1 Fixed patterning

Fixed patterning is an effect caused by the interaction of the GIS digital electronics with the analogue detector read-outs; it is very pronounced in some parts of the GIS spectra. Figure 3 shows a subset of data from detector 1, before and after smoothing.

It is necessary to remove the fixed patterning to allow further calibrations of the data, especially the gain depression calculations, which need to the number of counts per channel plate pore, i.e., before the fixed patterning corruption.
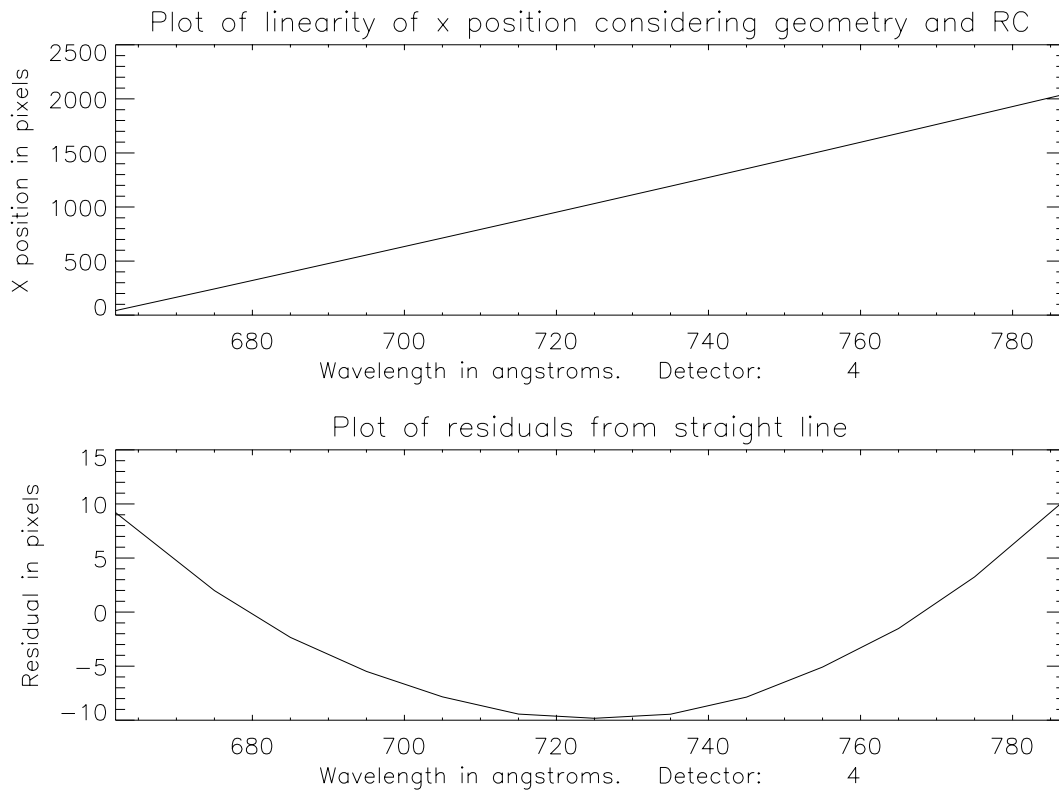
Figure 1. Error in wavelength calibration due to the geometry at detector 4.
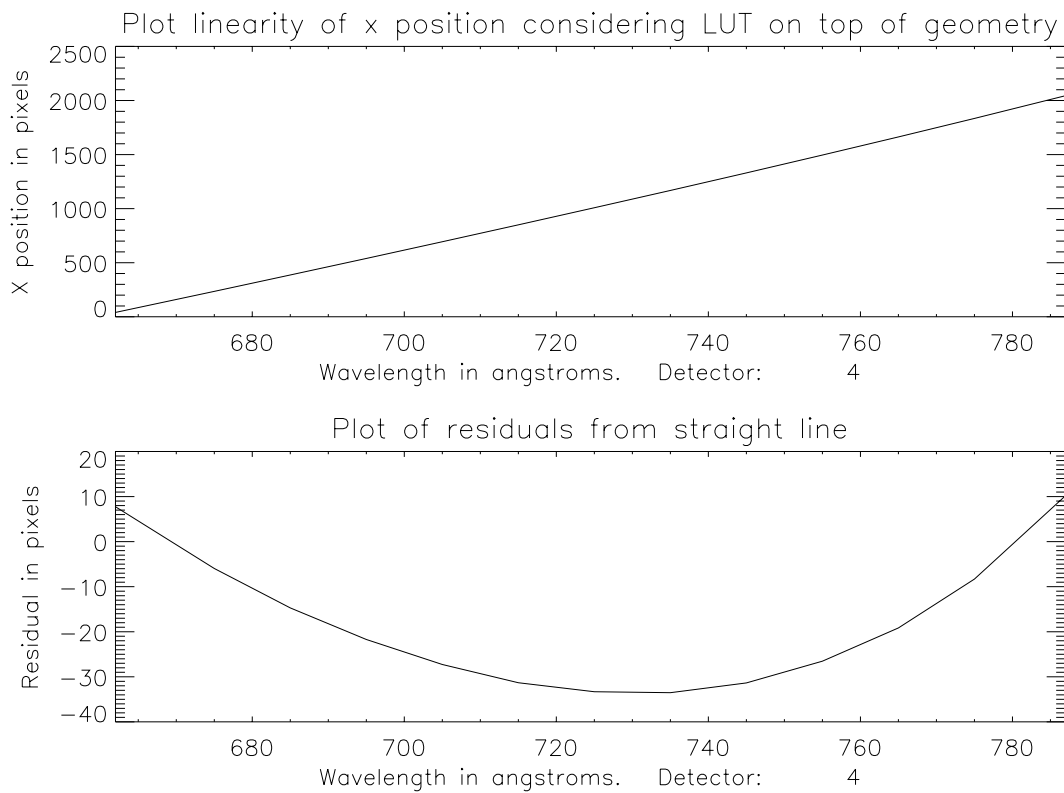
Figure 2. Non linearity in wavelength calibration.
This result is after combining the effects of LUT, geometry and the RC line positions.

3.1.1 Correcting for Fixed Patterning

A boxcar smooth of the data will reduce the fixed patterning seen in the figure but increase the line widths somewhat; the increase depending on the size of the boxcar used. Thus instead a convolution with a Hanning function is used in the program `gis_smooth`. This function preserves the total counts in the spectral lines, without introducing artefacts in the background. With the default setting the routine does not increase the line widths by more than 2%.

Inputs to the fixed patterning correction are the data to be corrected (the qlds), and an optional 'smoothsize'. The smoothsize is the size of the array containing the Hanning function, the default being '7'. To plot the function used by `gis_smooth`:

```
IDL> plot, hanning(7)
```

and substitute the number 7 with the size required. The variation of a gaussian fitted line at 188Å with 'smoothsize' can be seen in Table 1.

3.1.2 Errors in Wavelength

The *relative* wavelength position error introduced by fixed the fixed patterning itself is ±1 pixel (from ±0.03Å in detector 1 to ±0.06Å in detector 4), and considerably better after correcting using `gis_smooth`. This error is less than the *absolute* position errors of up to 10 pixels caused by the approximations used in the wavelength calibration.

3.1.3 Errors in Intensity

The intensity is not affected by fixed patterning, counts are simply displaced by up to one pixel either side of the intended position. The smoothing algorithm chosen does not change the intensities at all (see Table 1).

3.2 Ghosting

An effect in the GIS detectors is the presence of 'ghosts'. These are displaced spectral lines, or parts thereof, caused by an ambiguity in the encoding used by the electronics.

3.2.1 Correcting for Ghosting

The routine `ghost_buster` is used to remove or return ghosts in the GIS data.

When the GIS is in raw data mode, it transmits the data from one detector as a series of co-ordinate pairs from the detectors. When these co-ordinates are plotted they form a spiral (see the 'GIS Instrument Guide') where the spectral dimension lies along the length of the spiral, and the intensity is the number of counts at each position along the spiral. To translate these pairs into spectral position, the look up table (LUT) is used as part of the on-board GIS processing.

The ambiguity (or ghosting) in spectral data does not occur over the whole spectral range, but where the thin spiral arms broaden and overlap each other. If a spectral line is ghosted, it is confined to occur only at specific locations in adjacent spiral arms. It is these facts that are used in `ghost_buster`. The counts in a ghost must be added to the counts at the original location to produce the correct line intensity.
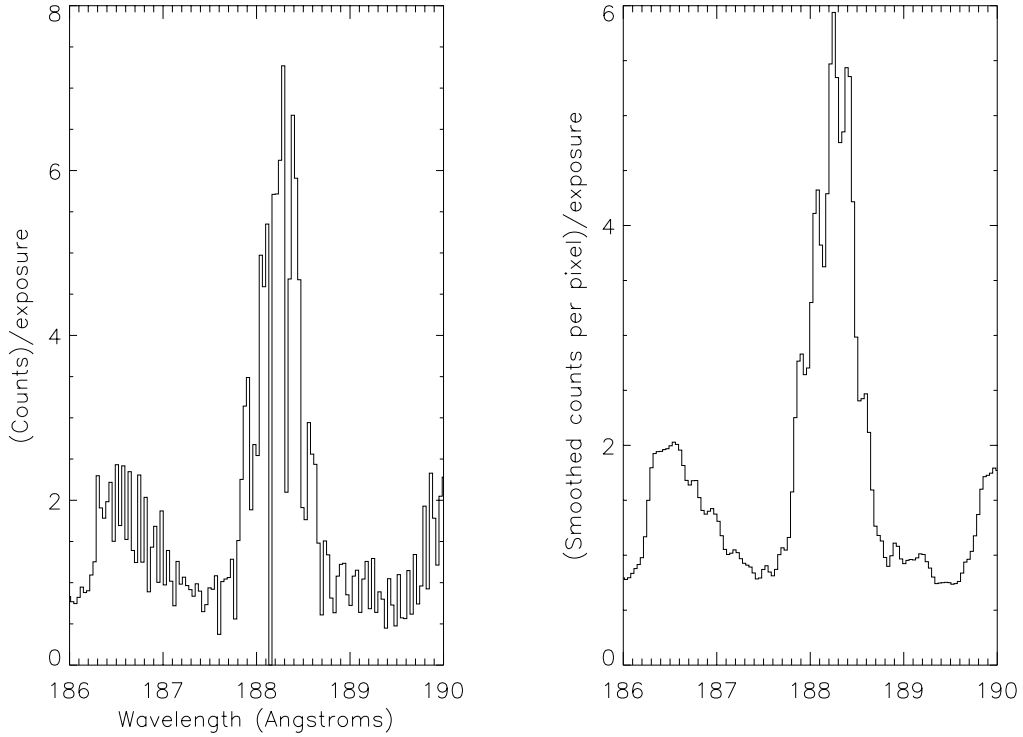
Figure 3. The effect of fixed patterning (left) and after smoothing with `gis_calib` (right). The default smoothsize (7) was used.

Smooth-size	height (counts/pix)	position (Å)	position (pixel)	1/e width (Å)	background	area (counts/s)
no smoothing	4.45761	188.259	1123.2	0.228531	0.853975	74.6082
4	4.43946	188.276	1123.7	0.229561	0.855614	74.6395
8	4.37399	188.275	1123.7	0.233065	0.855205	74.6611
12	4.26672	188.274	1123.7	0.239060	0.853971	74.7036
16	4.12166	188.273	1123.6	0.247343	0.855070	74.6641
20	3.94973	188.271	1123.6	0.257921	0.856862	74.6097
24	3.76101	188.270	1123.6	0.270797	0.858471	74.5914
28	3.56437	188.270	1123.5	0.285846	0.859894	74.6199
32	3.36759	188.269	1123.5	0.302877	0.860984	74.7009
36	3.17570	188.269	1123.5	0.321583	0.862542	74.7951
error	0.4	0.02		0.03	0.2	0.4

Table 1. Variation in fitted line parameters with size of smoothing.
This table was produced by fitting a single gaussian, with constant background, to the uncalibrated spectral line at 188Å. For each row in the table, a different 'smoothsize' was used in `gis_smooth`. The error quoted in the last row is the fitting error returned by the gaussian fitting. There is no discernible change in the fitting errors with smoothsize.

In ghosted areas, which cover 40% to 50% of the data, it is easier to separate the original line from ghosts where there are no blends. Thus ghosted areas in quiet sun observations are easier to correct than in an active region; although the unghosted areas remain unaffected for all observations.

3.2.2 Errors in Wavelength

`ghost_buster` assumes that the wavelength scale is linear when correcting for ghosts. This is not strictly true, the scale varies in a complex way closely approximating a quadratic. The deviations from linearity over small regions are negligible, thus `ghost_buster` will not allow single corrections to cover more than 100 pixels at a time (about 5% of the detector coverage). To cover a greater wavelength range, it is possible to apply as many corrections as necessary for each detector.

The error thus induced in the wavelength scale is small, at most ±0.5 pixels (0.015Å to 0.03 Å) due to rounding errors. Areas of the detector that have not had ghost corrections applied are not modified by `ghost_buster`.

3.2.3 Errors in Intensity

The routine `ghost_buster` deliberately preserves count rates when moving data, and thus the accuracy is only limited by the computer's floating point (single precision) accuracy. Again, areas of the detector that have not had ghost corrections applied are not modified by `ghost_buster`.

4. Line Widths and Profiles

The GIS line profiles are broader than expected, and in GIS detector 1 appear to have a peculiar profile. Figure 4 shows the average FWHM line widths for a number of selected lines on each detector. The expected line widths are from theoretical calculations with perfect optics, the 'stim' line widths are from very thin artificial lines stimulated by capacitive coupling on the detector backs.

From Figure 3, the profile of detector 1 lines can be seen, but with residual fixed patterning. To remove the fixed patterning entirely, with a small increase in line widths, the `smoothsize` keyword in `gis_smooth` can be increased from the default of 7.

It is likely that all detector profiles are double peaked, but with decreased spacing such that it is only noticeable in detector 1. The double peak may be due to a variation in line position as seen in calibration data taken at RAL before the launch[4]. This variation may also be responsible for the width of the lines as compared with the theory as shown in Figure 4.
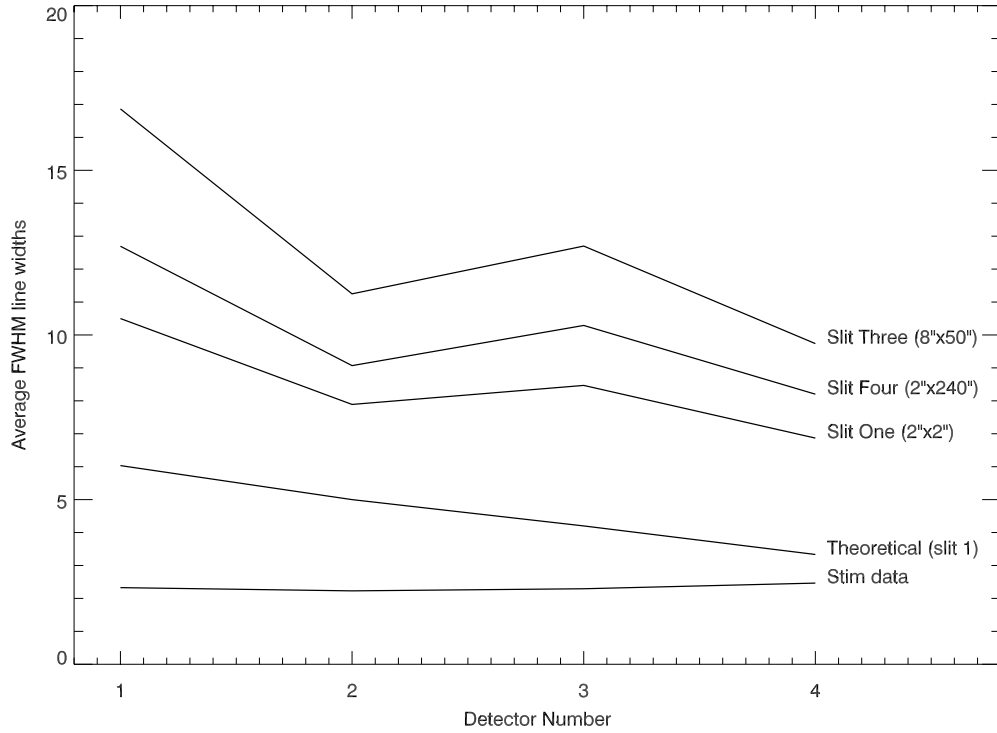
Figure 4. GIS line widths, assuming a gaussian profile.
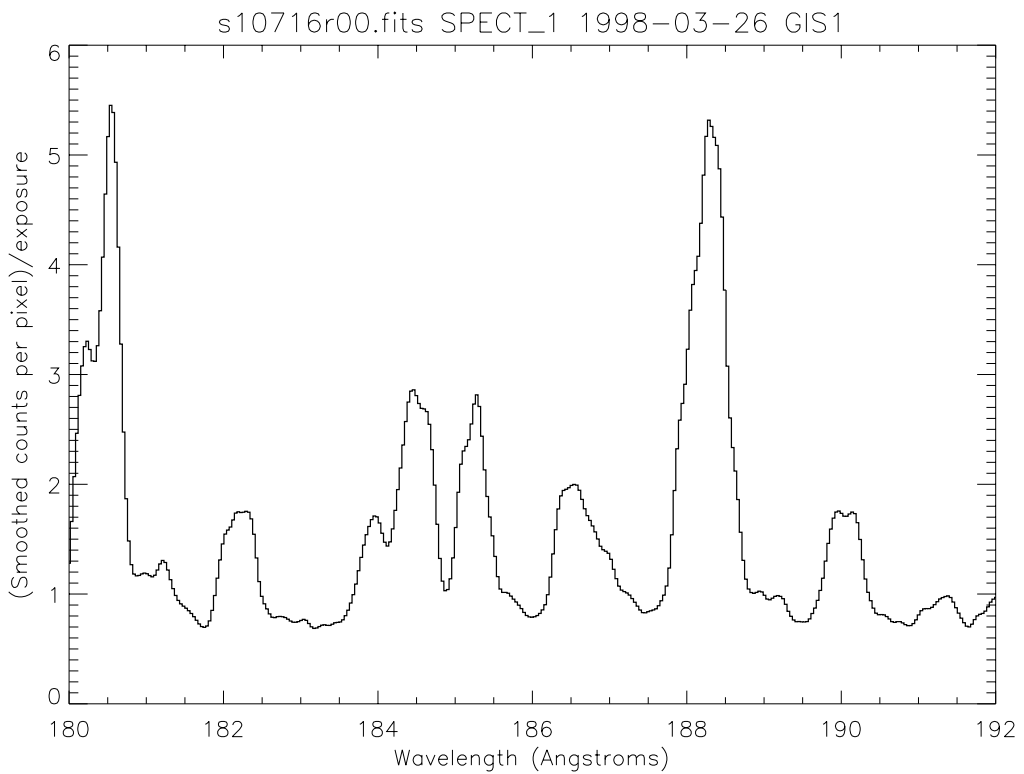
Figure 5. Data from the same observation as Figure 3, but with a larger 'smoothsize' (10).

5. Background and Flat Field

The measured pre-flight detector dark count is less than 12 counts per second per detector. The background seen in GIS observations is mainly due to scattered light from the telescope, particularly for detector 1. Detector 4 also shows solar continuum, especially at the long wavelength end. The normal data fitting procedures, by assuming a constant background when fitting over a small region of a detector, can be used to subtract the background. All detectors however, the show edge effects, caused by the high open electric fields at the extreme left and right edges of the detectors. This shows as a marked increase in the counts seen at these edges.

The sensitivity of the detectors vary across each detector, and the pre-flight sensitivities folded into the telescope sensitivity are used in the GIS calibration software (`gis_calib`). The routine `gis_write_calib` can be used to plot the current calibration coefficients. The high voltages on the GIS detectors are adjusted occasionally to maintain the average detector sensitivities with time. Section 7 below describes these routines in more detail.

Flat field observations are used to check *relative* changes in sensitivity across each detector. These special observations with the GIS doors closed and using filaments cannot test the absolute sensitivity of the detectors, nor can they compare the relative sensitivity of the four detectors to each other. They are only used to check for any variation in sensitivity from the pre-flight baseline.

The main cause of changes in sensitivity across detectors is gain depression in the micro-channel plates, where the gain in individual pores in the channel plates are reduced. The two forms of gain depression are 'short term' (i.e., count-rate dependant) and 'long term'.

5.1 Long Term Gain Depression (LTGD)

There are two problems here: One is the global decay of gain across the whole detector-caused by outgassing, plate ageing, filament usage, etc.; the other is differential decay caused by the fact that the spectrum is always illuminating the same parts of the detector.

The cause of this is simply usage of the detector micro-channel plates (MCPs). As charge is removed from the MCP channels, the gain is gradually reduced. This has the effect of reducing the apparent intensity of the line if the high voltage is not increased to compensate. For GIS, the parts of the detectors illuminated by bright lines will suffer first. Because of the wide range of intensities being viewed, it will not be possible to compensate for the LTGD in all lines at once by increasing the high voltage. A particularly intense line may cause gain depression in neighbouring regions up to a distance of 1 mm (2% of spectrum).
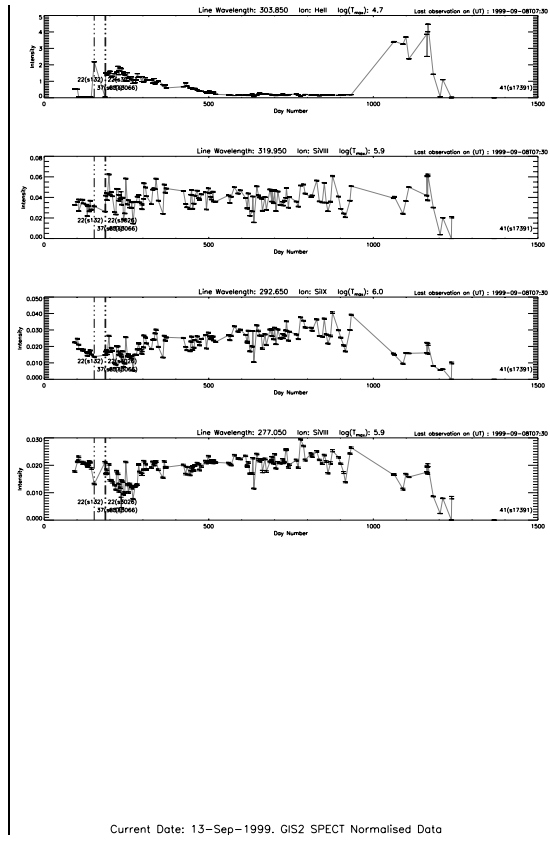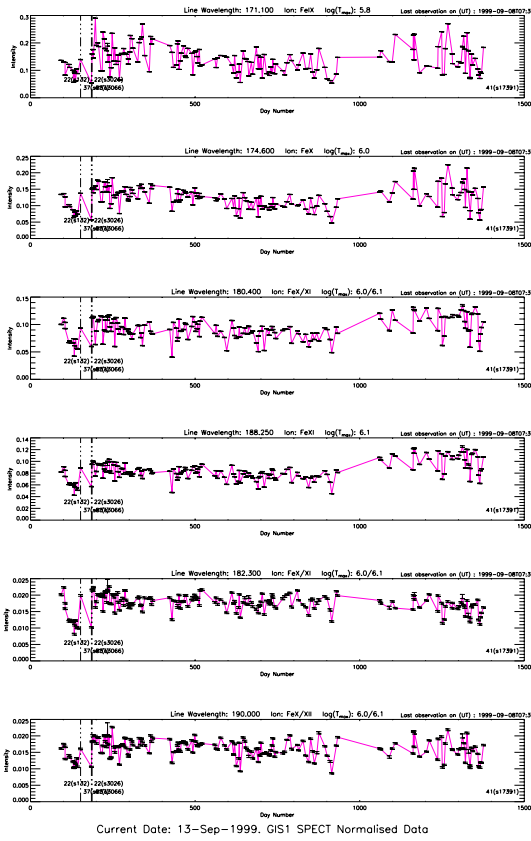
Figure 6. Variation in spectral line strengths in detectors 1 and 2.
This covers some of the brightest to faintest lines. Note that no observations have been made with detector 2 since about April 1999 (mission day 1250).
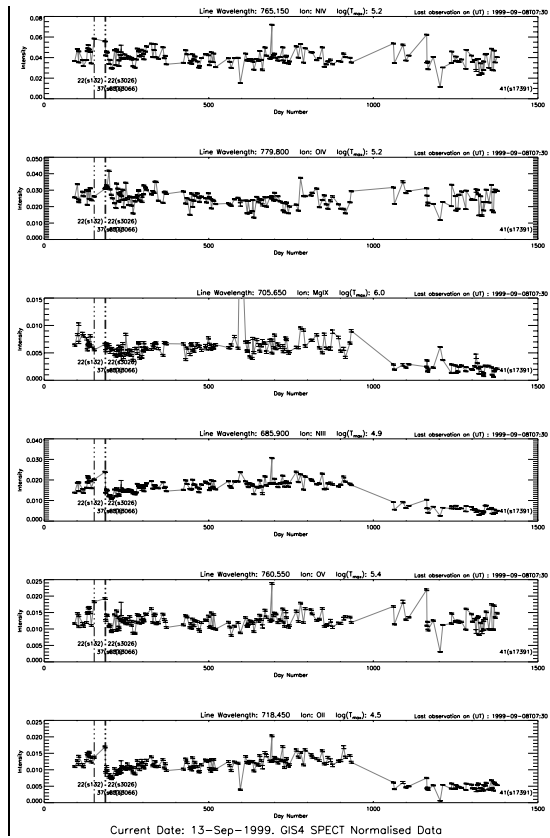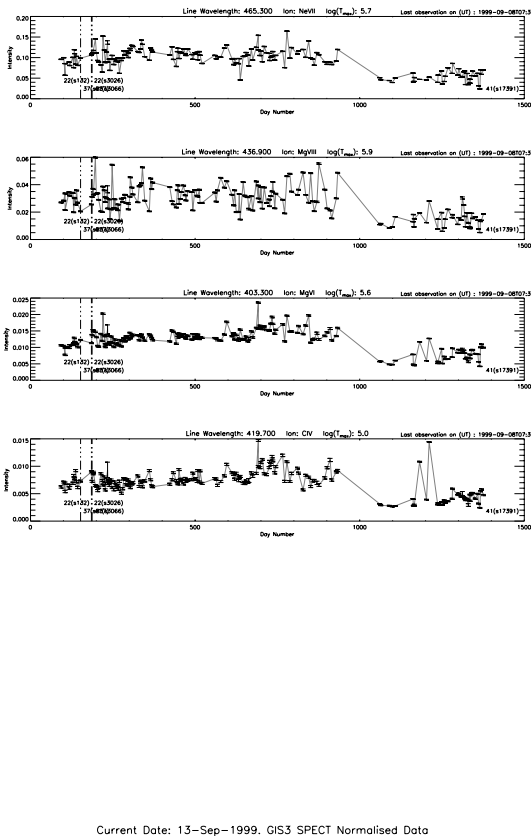
Figure 7. Variation of line strengths in detector 3 and 4.

Figure 8. Ratio of slit 3 to slit 1 intensities for detector 1, monitored over the whole mission.
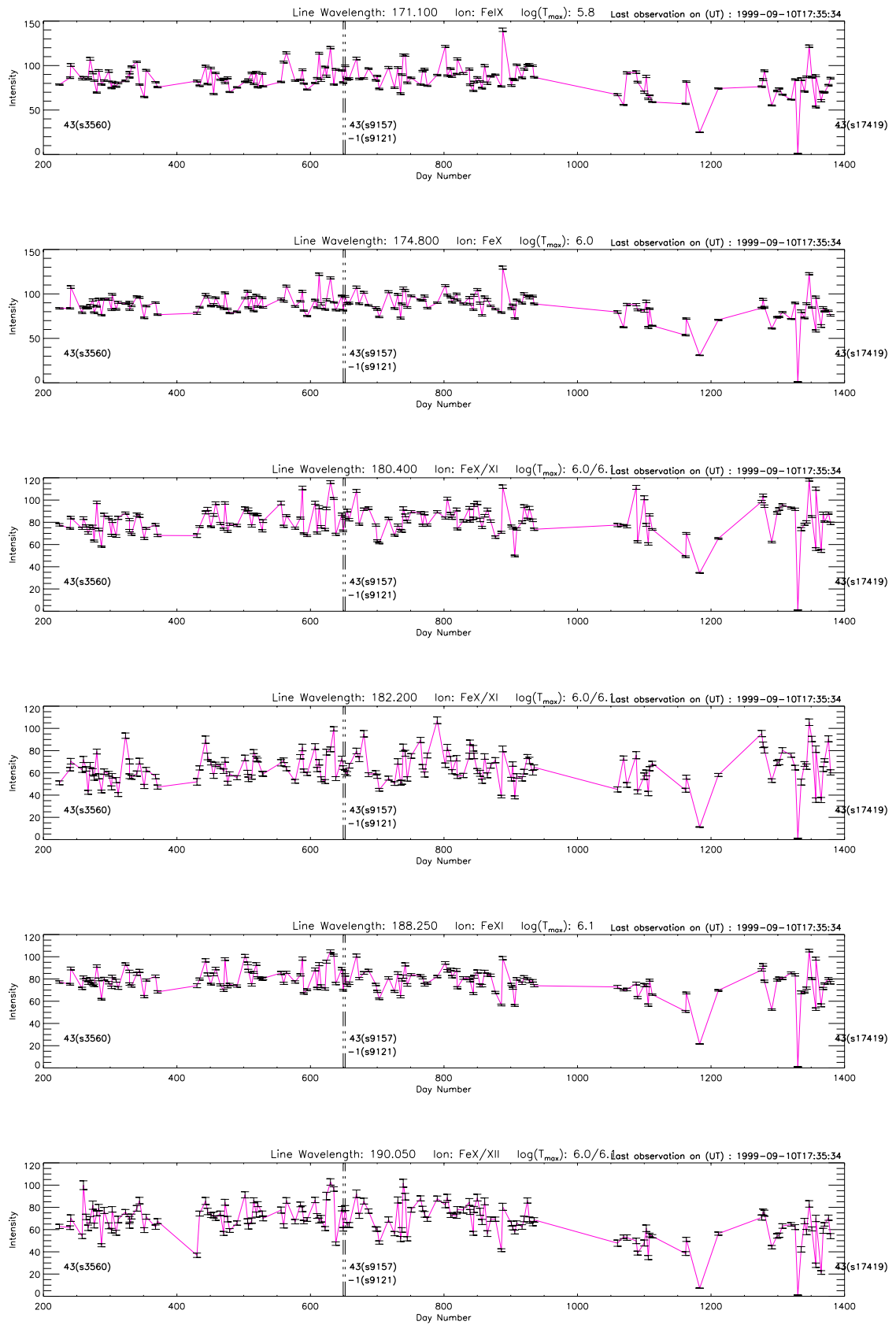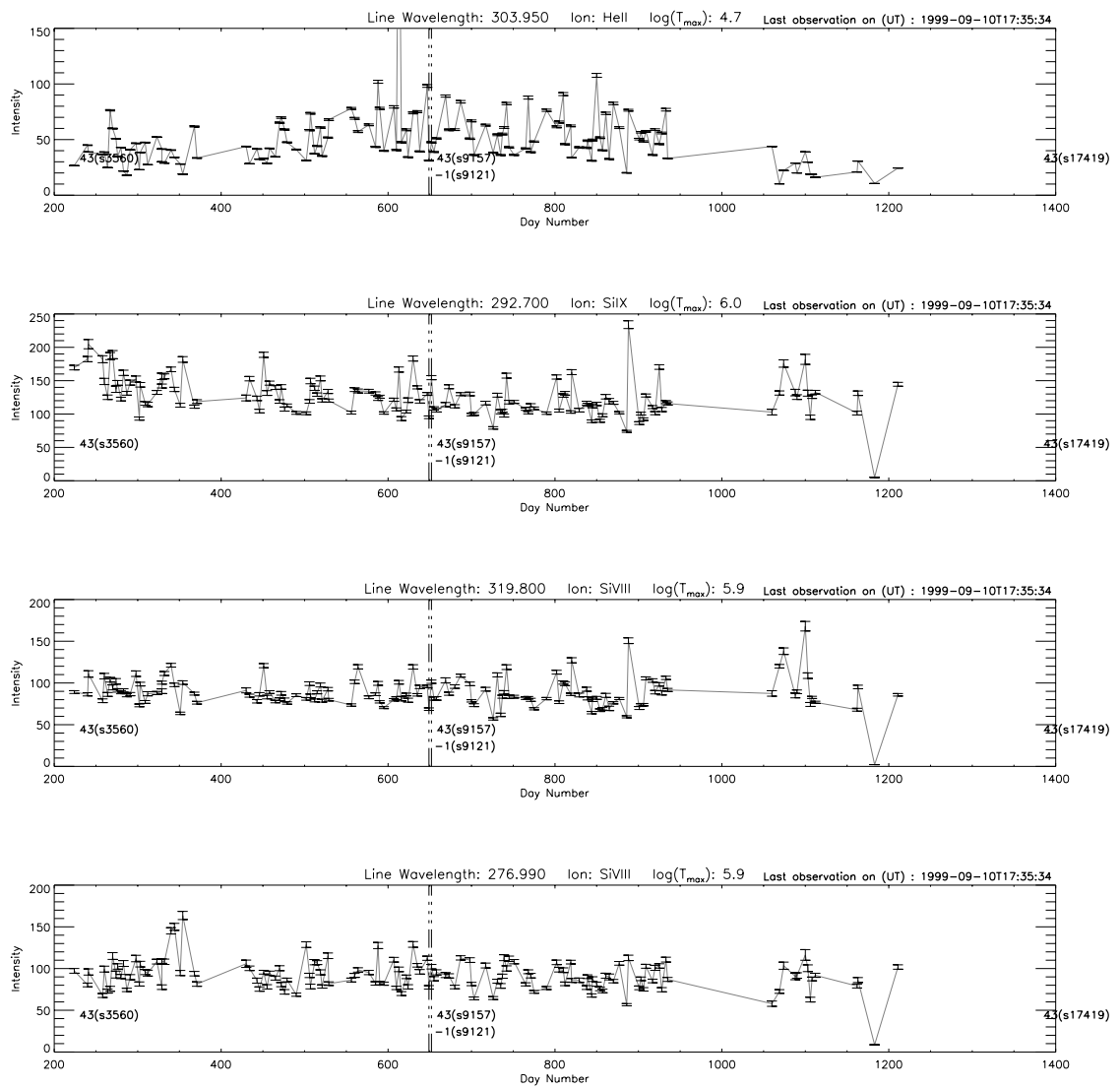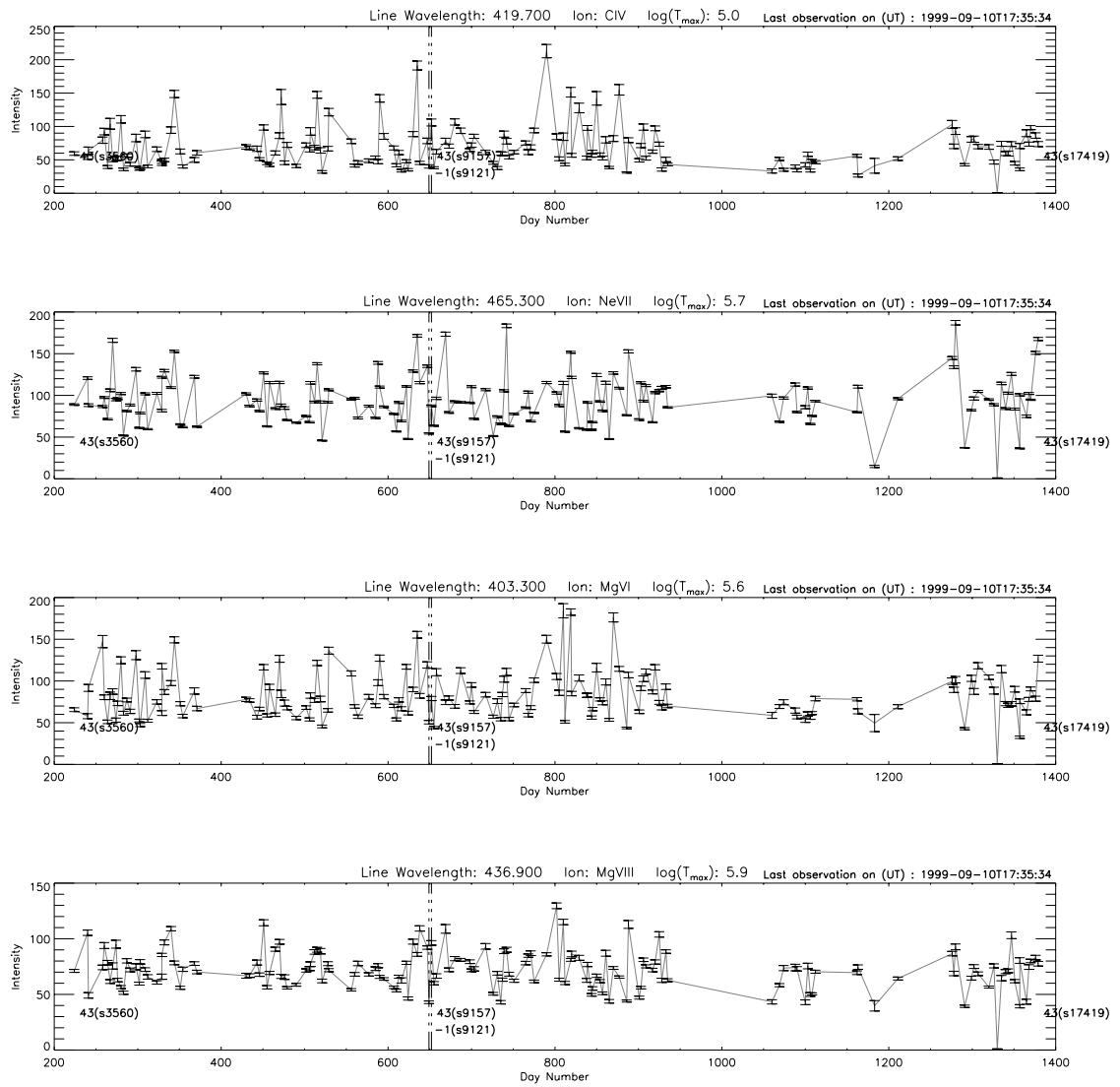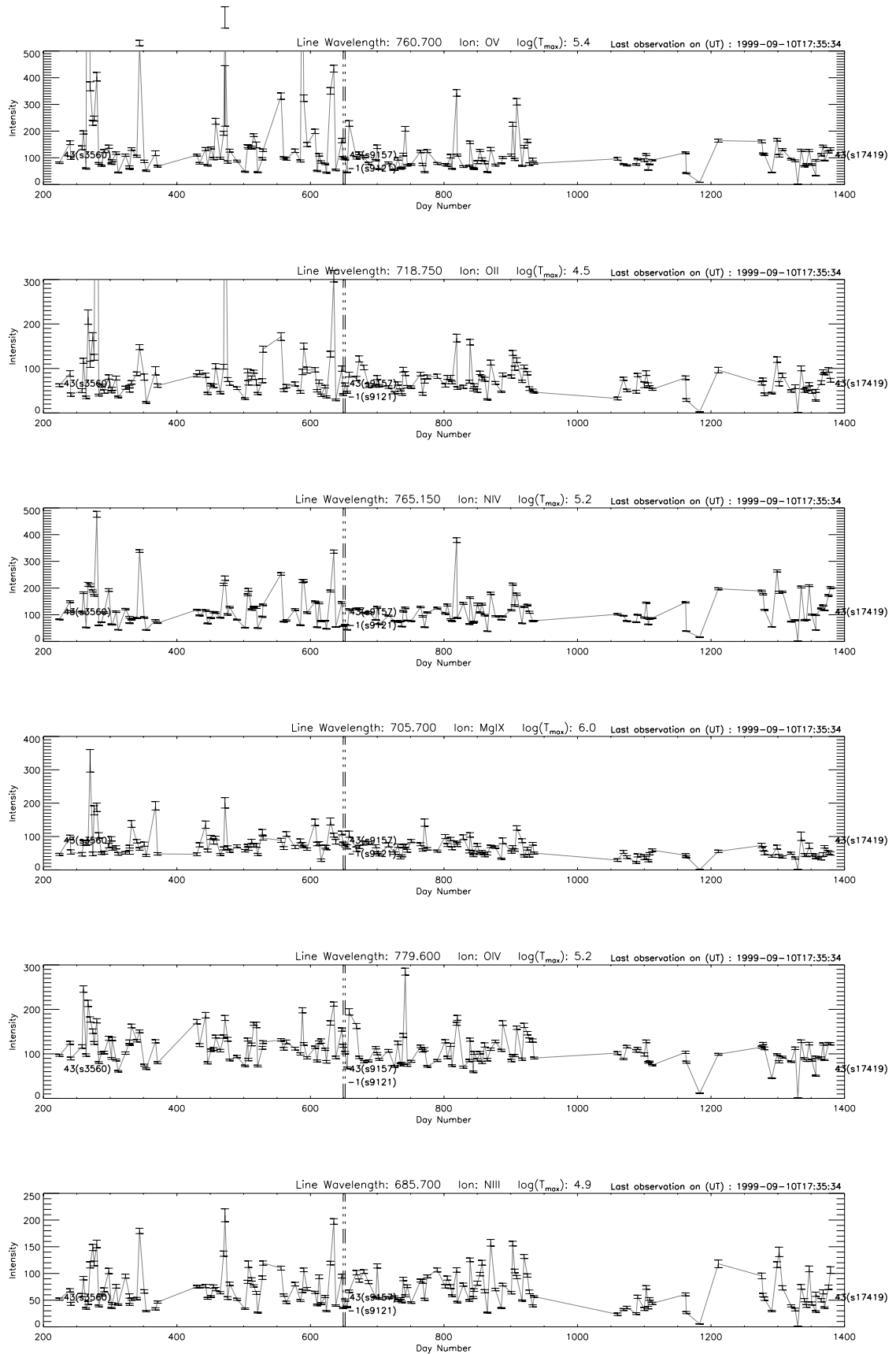
Current Date: 13-Sep-1999. GIS2 Slit3/Slit1 Ratio

Figure 9. Ratio of slit 3 to slit 1 intensities for detector 2, monitored over the whole mission.

Figure 10. Ratio of slit 3 to slit 1 intensities for detector 3, monitored over the whole mission.

Figure 11. Ratio of slit 3 to slit 1 intensities for detector 4, monitored over the whole mission.

We monitor global decay by using repeated quiet sun observations since the launch of SOHO. If quiet regions of the sun are considered to be stable, then any decrease in intensity can be monitored with regular viewing of quiet sun regions. The brightest and weakest lines are checked for changes in intensity over the whole mission; see Figure 6*f*.

Secondly, we monitor differential decay by using the quiet sun with narrow and wide slits. Differential decay should show up as dips in the wide slit image intensity; see Figure 8*f*.

5.1.1 Filament Data for gain depression

Two tungsten filaments are mounted in front of the four detectors in the optics bench. When a current is put through either of the two filaments, electrons are emitted. The number of electron are controlled by varying the current through the filaments.

The detector front face can be biased to ± 12 V. The -12 V setting is for normal use with the UV, repelling any background electrons. The $+12$ V setting is used to attract the filament electrons to the detectors.

The purpose of the filaments is to provide a repeatable and quick view across the each individual detector active area. They illuminate the whole of the front face, unlike a UV spectrum. Any regions suffering from gain depression will appear as a region of lower count rate. If the filament setting and detector settings are repeated identically after periods of use, changes in the detector performance can be monitored. It is also necessary to close the doors while the filament data is being taken, because there is no blank slit provided.

The approach taken is to compare the most recent filament measurement with one made at the start of the mission in order to determine the present local throughput.

The problem with using filaments to monitor global decay is that they do not stay constant in time. We currently set up the filament and the HV to give the same count rate over the whole detector. Then dividing one spectrum by the other, on a pixel by pixel basis, will give values equal to 1 in non-gain depressed regions, and more than 1 where there has been loss of sensitivity.

5.1.2 LTGD Correction

Long term gain depression and flat field data files can be used to compensate for such gain depression. These data can also be used to make adjustments for changes in detector response over the illuminated areas. These files are used automatically by the routine `gis_calib_ff_ltgd` which is called from `gis_calib`. The data files are time-stamped, and the file nearest in date to the observation is used.

Currently, no regions of LTGD have been seen in any of the detectors, with the exception of the region around the excessively bright HeII 304Å line (see Figure 6). Here the count rates have dropped by a factor of 50 or more since the launch of SOHO, and are considered uncalibratable. By default, the routine `gis_calib_HeII`, called from `gis_calib`, will mark the region around this line as uncalibratable.
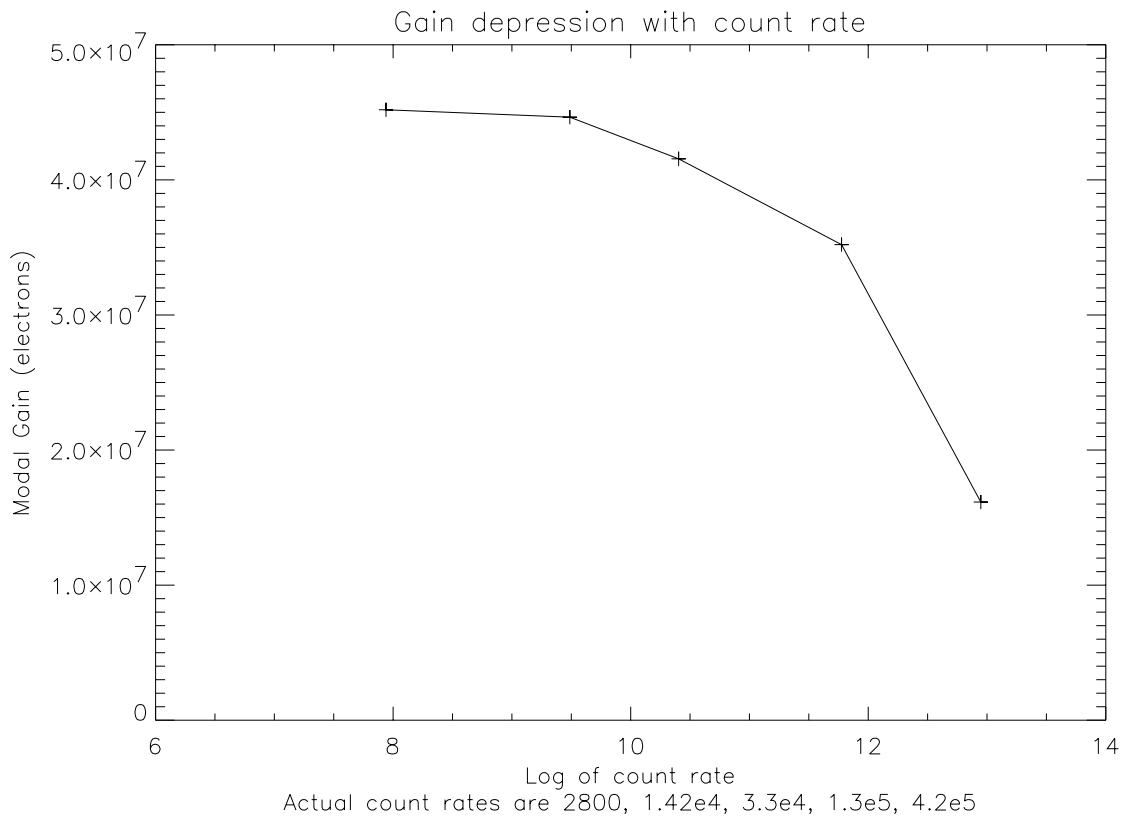
Figure 12. Reduction of gain with increasing input count rate.
From A. A. Breeveld (1996)[3].
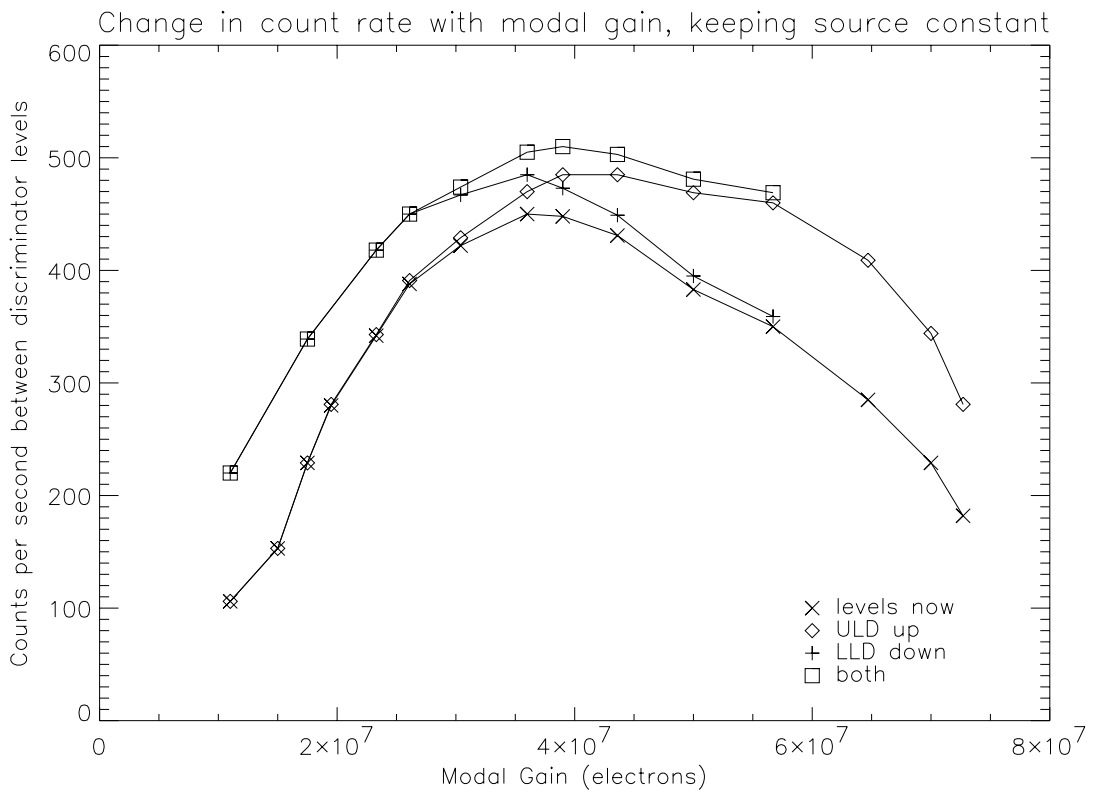
Figure 13. Stability of output count rate with changing gain.
From A. A. Breeveld (1996)[3].

5.1.3 Correction Errors

As no other regions of the detectors need LTGD correction, there is no correction implemented in the LTGD and flat field data files. Thus no errors in the intensity are introduced by this correction. Future corrections, if needed, will introduce a small error in the resulting intensity, depending on the accuracy of the filament data measurements.

5.2 Count Rate Dependent Gain Depression (CDGD)

This gain depression occurs when there is a high count rate in a region of the detector (such as occurs with a bright spectral line using a large slit) such that the MCP cannot recharge fast enough to provide full gain for every event; these events are discriminated against and thus the number of events are not counted accurately.

Since MCP gain is reduced as the local count rate is increased, the effective throughput at any part of the spectrum is a function of the local count rate.

5.2.1 Correction for CDGD

The routine `gis_calib_stgd` makes an estimate of the correction needed for count-rate dependent gain depression (also known as short term gain depression), but the accuracy of such a calculation is low. The correction is implemented on a pixel by pixel basis, but a limit of 4% correction is implemented in this software, if the correction needs to be greater then the datum for that pixel only is marked as uncalibratable.

The information used to calculate the amount of CDGD comes from A. A. Breeveld 1996[3] pages 139*ff*, where the change in gain is calculated as a function of input count rate per MCP pore. This is combined with *ibid.* pages 171*ff*, the change in output count rate as a function of gain. The relevant graphs are reproduced here as Figure 12*f*.

Finally, the number of pores illuminated for each slit is calculated from J. Lang *et al.* (1999) pages 41*ff*. For this to work, a valid approximation is made in which the positional resolution from the electronic readout is considered small compared with the spectral line width.

5.2.2 Errors in Intensity

As mentioned, the errors involved in calculating the amount of CDGD are potentially large, thus a 4% limit is set on the correction applied. This implies a maximum standard (1/e) error of around ±2% in the intensity of the brightest lines after correcting for CDGD. Lines that are too bright are marked uncalibratable.

5.3 Edge effects

Most detectors show edge effects, both as spikes and a gradual increase in the background. There are many causes for these effects, notably: a compression of the wavelength scale, causing an increase in the background; end spoiling in the microchannel plates, where the strong electric fields diverge at the ends of the detectors; changes in the solar background, mainly from the HeII continuum; and some very bright (solar) lines, seen especially in detector 2. Work is continuing on calibrating the non-solar effects.
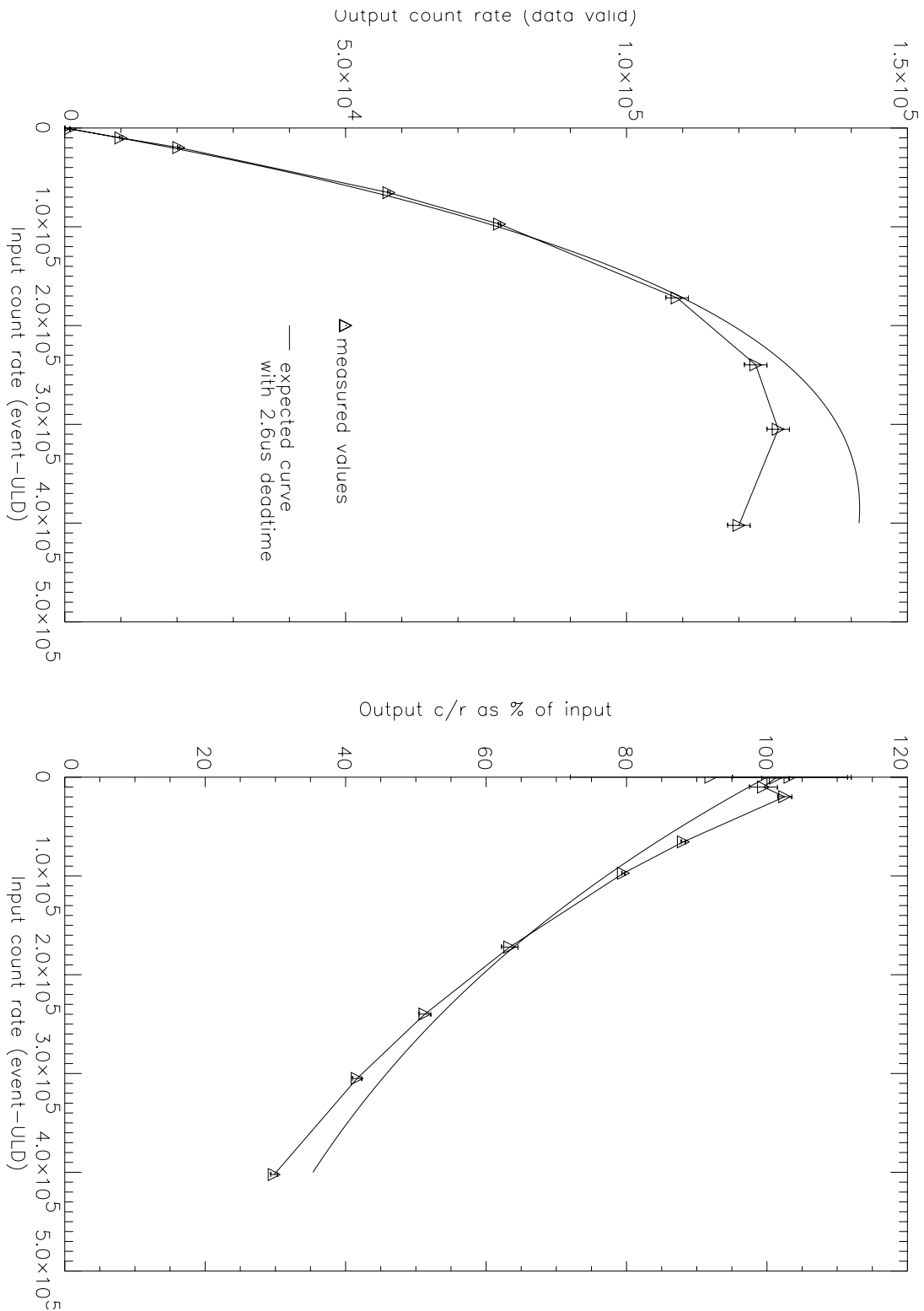
Figure 14. Plot of relationship between the analogue circuit output and input count rates.

The dead time used in the fit is 2.6 μs. The curve rolls over at higher count rates leading to a reduction in output count rate at very high input count rates.

Variations in the intensity of the edge effects are seemingly random - there is no obvious correlation with solar position or region observed. The change in wavelength scale seems constant, and will be incorporated into the calibration.

6. Electronics Calibration

There are three main sources of electronic dead time corrections needed, these are: FIFO dead time; Quiz-show dead time, and analogue dead time.

6.1 FIFO dead time

The dead time is a straightforward correction for an on-board First In First Out (FIFO) event queuing chip. It applies to all four detectors simultaneously, and involves a constant non extending dead time allowing 10^5 counts per second through unhindered, with small corrections for higher rates.

6.2 Quiz Show dead time and maximum burst rate

This is associated with combining the data from the four detectors into one stream and the limited rate of data flow to the CDHS. This method of choosing the events results in a global dead time but, as with the analogue dead time, does not affect the distribution of events. The programmed Quiz-show correction is simply an upper limit on the rates; if photon events are less than 6 microseconds apart then the data are marked as uncalibratable. The maximum rate is then $1.0/(6.0 \times 10^{-6})$ or approximately 1.7×10^5 counts per second over all four detectors.

In fact the count rate is ultimately limited by the rate at which information can be sent to the CDHS from the GIS box, which is 8.9×10^4 c/sec. A FIFO buffer, 512 events deep, is used to store bursts of events closer together, allowing short bursts of events at a higher count rate. At total (sum of all four detectors) count rates near to this value it may be possible to reduce the number of detectors being used. If the count rate from just one detector is still too high, the intensities must be treated with caution, the calibration software marks such data as uncalibratable.

6.2.1 Errors in Intensity

Count rates in excess of the limits imposed by the quiz show processing are marked as uncalibratable by the calibration software (`gis_calib_quiz`)

6.3 Analogue dead time

This involves an extending dead time of approximately 2½ microseconds. The data used to correct for this were measured before launch using the flight electronics and plotted in Figure 14. The routine `gis_calib_analogue` reads this information from the data file `$CDS_GIS_CAL_INT/deadtime.dat`.

The dead time used in the fit is 2.6 µs. The curve rolls over at higher count rates leading to a reduction in output count rate at very high input count rates. After the arrival and detection of a photon there follows a finite time before a new event can be detected, within which any new events will be discarded by the electronics pile up discrimination. This limits the rate at which events may be detected and results in a non-linear relationship between the input and output count rates. The reduction of the

global count rate of the detector can be calculated and therefore compensated for. Provided there is no rapid change in the input image, this dead time does not alter the distribution of detected events in the output image. Every 'pixel' is available to detect a new photon within the same time period-the length of the period is reduced by dead time by the same amount for each pixel. i.e., the detection of a photon depends only on its arrival time, not on its position.

6.3.1 Errors in Intensity

At low count rates the calibration is linear, and with little error. The quiz-show correction derailed in section 6.2 limits the count rates such that there is no error in intensity introduced by this correction.

6.4 Other intensity effects

Data from the GIS are transmitted to the on-board data handling system (CDHS) on an event by event basis. The dead times and limits associated with the event data are discussed above. I will now discuss other effects that can occasionally be seen in the data.

The GIS events are integrated in the CDHS. These counters are limited to 16 bits per spectral bin, and if the integration times are excessively long the counters will fill (but not wrap). It would take an exposure time of approximately a few hours on the quiet sun with the 4"×4" slit, and correspondingly less in active regions and for larger slits. Thus a little care must be taken to use short exposure times, no more than a few minutes, when making such observations.

When CDS data is transmitted to the ground, and from the ground antennas to the processing facility at Goddard, there is a possibility of data loss. Such missing data is signified in the GIS and NIS data as a negative value for those pixels. Some routines exist (e.g., `cds_fill_missing`) to guess the missing values, but some care must be taken with the results. Much lost data is 'recoverable' and will be restored from CDROMs processed at Goddard within a few months of the observation.

6.4.1 Errors in Intensity

Missing data introduces obvious errors in the data - such points are marked with negative values and should not be used for analysis. Full spectral bins are marked with the value '65535', and should not be used either.

7. Effective Area and Detector Sensitivity

After all the above corrections have been applied, we can optionally apply the best known absolute calibration data, using `gis_calib` with `/steradian_m2` or `/arcsec2_cm2` switches. Detailed use of the `gis_calib` program can be found in the GIS Software User Manual[2].

The GIS calibration coefficients used are those from the RAL pre-flight calibration tests[4], the coefficients can be viewed graphically using the IDL program

```
IDL> .run gis_write_calib
```

and are shown in Table 2.

7.1 Comparison with flight data

The calculations are based on a ground based calibration exercise for the whole of CDS. The relative calibration coefficients have since been verified in flight[5], but please note that there is currently a very large uncertainty in the absolute values.

Every month, as the CDS part of the SOHO-wide INTERCAL programme, GIS observations are made along with NIS at similar (but not exactly the same) time periods and areas of the sun. It is impossible to run the GIS and NIS simultaneously. Unfortunately, comparison of GIS and NIS data do not show consistent cross calibration; variations of factors of 2 to 5 can be seen in the calibrated NIS to GIS data ratios. This is probably due to large solar variability at transition region and coronal temperatures, both spatially and temporally, see Table 3.

7.2 Errors in Intensity

The errors in the absolute intensities is difficult to estimate. The ground calibration errors are relatively small, about 25% or better (Table 14 in the Laboratory Calibration paper[4]). Absolute calibrations may be incorrect by factors of 2 or more, although the GIS detectors are stable with time, see section 5.1.

Base efficiencies (counts/photon)	G1	G2	G3	G4
	1.71200E-04	1.99400E-04	2.86000E-04	9.56000E-05

Wavelength dependence of the efficiencies	x^0	x^1	x^2	x^3
G1 polynomial	-2.31180E+01	3.88640E-01	-2.03520E-03	3.47200E-06
G2 polynomial	1.10400E+02	-1.13200E+00	3.85060E-03	-4.30720E-06
G3 polynomial	1.43580E+00	-1.00310E-03		
G4 polynomial	1.22100E-01	1.19410E-03		

Effective area (cm^2)			
Average area:	2.51667E+01		

Vignetting against mirror position (cm^2)	x^0	x^1	x^2
Polynomial	2.34380E+01	3.38890E-02	-1.38890E-04

Table 2. Calibration coefficients used in `gis_calib_area`

```
Date Observed: 1997-02-02
NIS studies:  s6868r00 s6866r00 s6864r00 s6862r00
GIS studies:  s6869r00 s6867r00 s6865r00 s6863r00

NIS label:  MG_8_317_01
 NIS =    3.1890      GIS =    6.5704
 Units: Photons/second/pixel/arcsec^2/cm^2

 Ratio NIS/GIS =        0.49

NIS label: FE_13_320_80
 NIS =    1.5765      GIS =    3.8453
 Units: Photons/second/pixel/arcsec^2/cm^2

 Ratio NIS/GIS =        0.41




Date Observed: 1998-05-01
NIS studies:  s10989r00 s10987r00 s10985r00 s10983r00
GIS studies:  s10988r00 s10986r00 s10984r00 s10982r00

NIS label:  MG_8_317_01
 NIS =    7.0867      GIS =   41.9338
 Units: Photons/second/pixel/arcsec^2/cm^2

 Ratio NIS/GIS =        0.21


NIS label: FE_13_320_80
 NIS =    3.6808      GIS =   24.6605
 Units: Photons/second/pixel/arcsec^2/cm^2

 Ratio NIS/GIS =        0.19
```

Table 3. Variation of NIS and GIS data ratios using INTERCAL observations. The above observations were selected to show the wide variation in the comparison of NIS and GIS data. The two observations were made on quiet regions of the sun, and the calibrated intensities show large absolute and relative variations between 1997 and 1998. The lines observed were Mg VIII 317Å ($\log_{10}(\max(T_e))$=5.9) and Fe XIII 320Å ($\log_{10}(\max(T_e))$=6.2).

8. References

[1] R. D. Bentley (1999);
CDS Software note 54: GIS Instrument Guide.

[2] E. R. Breeveld (1999);
CDS Software note 55: GIS Software User Manual.

[3] A. Breeveld (1996);
PhD Thesis, Ultraviolet Detectors for Solar Observations on the SOHO Spacecraft, University of London.

[4] J. Lang *et al.* (1999);
The Laboratory Calibration of the SOHO Coronal Diagnostic Spectrometer, RAL Technical Report RAL-TR-1999-036. Also in the Journal of Optics A (*in press*).

[5] Landi, E., Del Zanna, G., Breeveld, E. R., Landini, M., Bromage, B.J.I., Pike, C.D.: (1999);
Relative Intensity Calibration of CDS-GIS Detectors on SOHO using a Plasma Diagnostic Technique, Astronomy and Astrophysics Supplement, v.135, p.171-185